DINAME 2023 - Proceedings of the XIX International Symposium on Dynamic Problems of Mechanics,
A.S. De Paula, A.T. Fabro and M.R. Machado (Editors), ABCM.
Pirenópolis, Go, Brazil, February 26th to March 3rd, 2023

Data Compatibility Check of an UAS With a Flexible Wing

Souza A. G.[1], Castillo-Zúñiga, D. F.[2], Sarmento A. G. P.[3], Machado R. C.[4], Silva G. A. R.[3] and Góes L. C. S.[3]

[1] IDMEC, Instituto Superior Técnico, Universidade de Lisboa, Av. Rovisco Pais, No. 1, 1049-001 Lisboa, Portugal

[2] UNESP, Faculdade de Engenharia, Câmpus de São João da Boa Vista, 13876-750, Av. Profª Isette Corrêa Fontão, 505 - Jardim das Flores - São João da Boa Vista

[3] Instituto Tecnológico de Aeronáutica, 12228-900, São José dos Campos, Brasil.

[4] UNESP, Faculdade de Engenharia e Ciências, Câmpus de Guaratinguetá, 12516-410, Av. Ariberto Pereira da Cunha, 333 - Portal das Colinas - Guaratinguetá, Brasil

Abstract: This paper discusses the means of checking and improving the quality of flight-recorded data during the flight test campaign of the unmanned aircraft system (UAS) called Éolo. The UAS has a high aspect ratio and structural flexibility, designed to study aeroelastic phenomena and evaluate the interaction of the structural flexibility effects with the flight dynamics of the aircraft. To quantify the instrumentation errors and to correct the measured data from the sensors, a Flight Path Reconstruction (FPR) has been developed. The FPR is based on estimating the sensor error parameters using the aircraft kinematic equations and inertial measurement unit (INS/GNSS) readings as inputs. Furthermore, the initial conditions can be obtained from smoothed measurements at the initial time. This paper describes the flight test procedure used to obtain the flight data, design the FRP and perform the data analyses in order to obtain the most accurate flight data for the identification process. The paper is based on part of an ongoing research project.

Keywords: UAS; Flight Path Reconstruction; Flight Test; Aircraft Flight Dynamics; Instrumentation Errors; Bias Estimation

1 INTRODUCTION

The data collected in flight tests need to be accurate to guarantee the numerical representation of the observed dynamics and kinematic consistency of the aircraft flight. The application of data compatibility checks to determine the scale and bias of the flight sensors is necessary before further parameter identification studies can be realized ”de Oliveira Silva (2011)”. The data compatibility check is a procedure that has the objective to quantify the instrumentation errors and correct the measured data for systematic errors like scale factor, zero shift biases, and time lags.

The analytical modeling of aircraft aerodynamic parameters is too complex, and not complete enough to represent all the real system disturbances, and to complete the real aircraft model accurately it is necessary to make experimental modeling using inverse problem with real flight data ”**?**”. Experimental aircraft modeling consists to construct a prototype, make flight tests with specific inputs, and accurately observe the dynamic responses of the system. These responses are registered and compared with simulated data of the aircraft model, to effectively validate the model with real flight data. The model parameters are determined by an identification procedure. In this process, it is necessary to have accurate measurements of aircraft response. Using the validated measurement data and analytical models in an optimization method is possible to estimate the unknown parameters ”de Oliveira Silva and Mönnich (2012)”. For this procedure is important that the measurement data is properly verified and corrected ”Barbosa and Góes (2018)”.

Before the realization of the aircraft identification process, it is important to assure the trustworthiness of the measurement given by the flight sensors, because these measurement data are susceptible to many different interfering and modifying effects, and if not correctly accounted for, can destabilize the system response when it is inside a closed-loop system ”Martínez *et al.* (2020)”, ”De Silva *et al.* (2010)”, ”Theis *et al.* (2015)”.

A common procedure to improve measurement accuracy is the ”data compatibility check”, a method to reconstruct the flight path (FPR) using the onboard sensor data as inputs to the nonlinear aircraft kinematic equations. The integration of the nonlinear state space equations describing the aircraft kinematic equations, to obtain the vector of observed outputs attitude allows for the verification of consistency between the observed and predicted output variables Dias (2014). The procedure can also be used to estimate the error model of the sensors, such as the systematic errors of the sensors, bias drift, and scale factors.

The paper proposes to describe the flight test procedure used to obtain the flight data, implement the FRP and make the data analyses in a way to improve the accuracy of flight data for the posterior aerodynamic parameters identification procedure.

The UAS has its properties and particularities described in the first part of this paper. The next part shows the FPR procedure that includes the mathematical equations that represent the kinematic movement of the UAS. A brief comment on the in-flight test design (The design procedure is further detailed in Zúñiga *et al.* (2019a)) and the flight test execution,

in the data flight section. In the next section, the output error method (OEM) is described with the purpose to estimate some states and the biases, and the scale factor. The following section presents the computational analysis and simulations. The last section presents the conclusion of this study with some future work proposals for this research.

1.1 Eolo - UAS

The Eolo UAS was developed by Flight Technologies and ACS Aviation Solutions, with the aim to study experimental aeroelastic instabilities as well as the observation of linear and/or nonlinear elastic effects in flight dynamics Souza *et al.* (2019).

The mass proprieties and the geometry characteristic are expressed in Table (1). The mass proprieties were validated in the measurement of mass proprieties laboratory at the Institute of Aeronautics and Space (IAE). The body of the Eolo was fabricated with expanded polystyrene foam and coated with carbon, for the wing structure has a main stringer with layers and fibreglass and expanded PVC Zúñiga *et al.* (2019b) Souza *et al.* (2019).

Table 1 – Geometry and mass parameters.

Parameters	Symbol	Values
Wing area	S	0.85 m^2
Wing mean chord	$\bar{c}$	0.23 m
Wing span	b	4.00 m
Aspect ratio		18.90
Fuselage length		1.89 m
Wing mass	m_w	2.00 kg
Total mass	m_t	8.87 kg
X Inertial moment	I_{xx}	2.53 kg m^2
Y Inertial moment	I_{yy}	1.60 kg m^2
Z Inertial moment	I_{zz}	3.96 kg m^2

The Eolo UAS has a specialized data acquisition system composed of internal and external sensors. The internal sensor is an inertial measurement unit (IMU) mounted on the CG of the UAS and the external sensors are: 19 accelerometers (ADLX345 with 16 g range, a bandwidth of 1600 Hz) distributed along the wing, in the fuselage it has 2 accelerometers (ADLX345 with 16 g range, a bandwidth of 1600 Hz), in the tail more 4 accelerometers (ADLX345 with 16 g range, a bandwidth of 1600 Hz), three linear strain gauges (CEA-06-250UR-350) positioned at the left side of the wing and a strain gauge rosette (CEA-06-125UW-350) near to the root of left semi-wing, a GNSS, a pitot tube and Alpha-Beta Vane. The position of each sensor is shown in Figure (1).

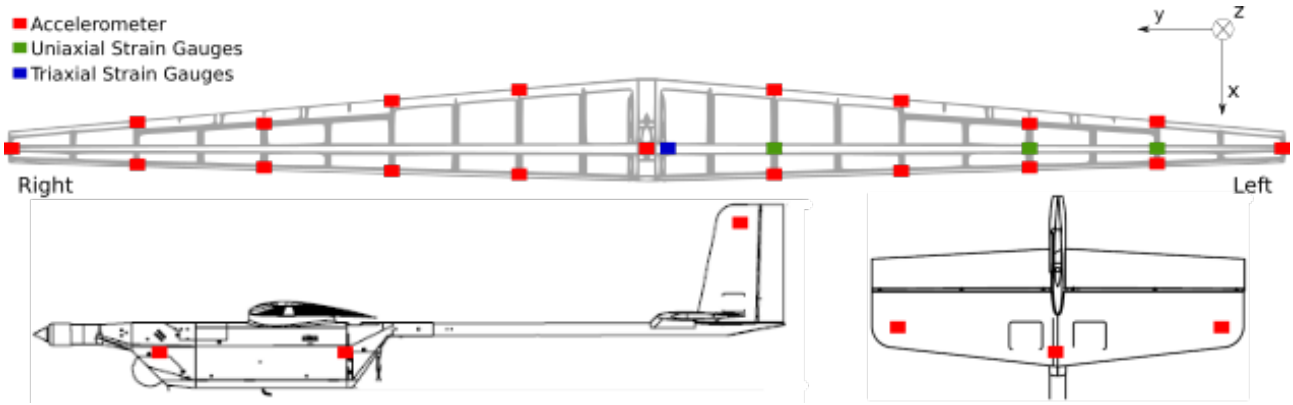

Figure 1 – External sensors positions.

2 FLIGHT RECONSTRUCTION PATH (FPR)

The Flight Reconstruction Path (FPR) is a way to verify the data collected by the sensors de Oliveira Silva (2011). The interpretation of the results of the FPR has an important role in the Data Compatibility Check because with this procedure is possible to extract important information about the sensors like systematic errors, quality of the signal etc.

The procedure of the FPR is exactly what its name says, is reconstruct the flight path using the data collected by the sensors, in special by the inertial sensors de Oliveira Silva (2011). Then to make the FPR is necessary to propagate the kinematic equations using the sensors data and estimate the bias of the sensors and the Euler angles (θ, ϕ and ψ).

2.1 Mathematical Model

For the FPR is necessary the kinematic model of the UAS and the equations that describe angles of attack α and sideslip β, the true airspeed V, and dynamic pressure $\bar{q}$.

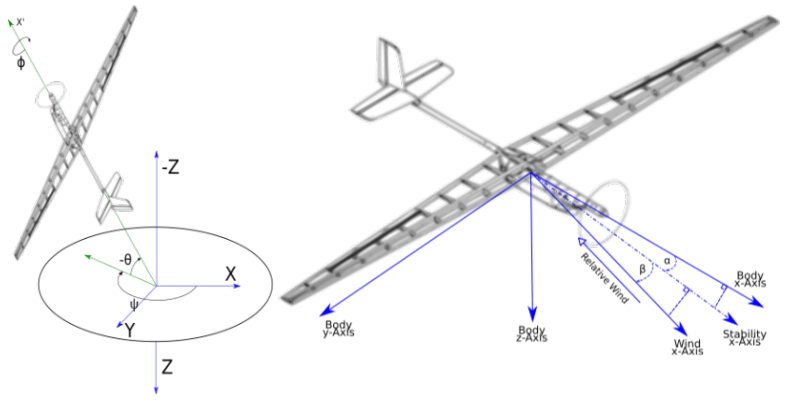

Figure 2 – System of references in the inertial referential frame, body-fixed axes and wind axes.

Figure (2), shows the reference systems that were adopted.

The kinematic model is derived from the equations of the translational motion of an aircraft. In the first case, it is assumed that the UAS is a rigid body Martínez *et al.* (2020) Souza *et al.* (2019) then the translational equations in the body-fixed axes system with origin in the gravity centre are given by:

$$\begin{aligned} m(\dot{u}+qw-rv)+mg\sin(\theta) &= F_x \\ m(\dot{v}+ru-pw)+mg\cos(\theta)\sin(\phi) &= F_y \\ m(\dot{w}+pv-qu)+mg\cos(\theta)\cos(\phi) &= F_z \end{aligned} \tag{1}$$

where F_x, F_y and F_z are the aerodynamic and thrust forces and ϕ, θ denote the roll and pitch angles.

The Eq. (1) can be rewrite in function of the axial acceleration a_x, a_y and a_z Souza *et al.* (2019) Waszak and Schmidt (1988),

$$\begin{aligned} \dot{u} &= a_x - qw + rv - g\sin(\theta) \\ \dot{v} &= a_y - ru + pw + g\cos(\theta)\sin(\phi) \\ \dot{w} &= a_z - pv + qu + g\cos(\theta)\cos(\phi) \end{aligned} \tag{2}$$

The rotation kinematic de Oliveira Silva and Mönnich (2012) Pfifer and Danowsky (2016) Souza *et al.* (2019) in function of the Euler angles ϕ, θ and ψ to the body-fixed rotations rates p, q and r is given by:

$$\begin{aligned} \dot{\theta} &= q\cos(\phi) - r\sin(\phi) \\ \dot{\phi} &= p + q\sin(\phi)\tan(\theta) + r\cos(phi)\tan(\theta) \\ \dot{\psi} &= q\sin(\phi)\sec(\theta) + r\cos(\phi)\sec(\theta) \end{aligned} \tag{3}$$

The position kinematics,

$$\begin{aligned} \dot{x}_E &= u\cos(\psi)\cos(\theta) + v(\cos(\psi)\sin(\theta)\sin(\phi) - \sin(\psi)\cos(\phi)) + w(\cos(\psi)\sin(\theta)\cos(\phi) + \sin(\psi)\sin(\phi)) \\ \dot{y}_E &= u\sin(\psi)\cos(\theta) + v(\sin(\psi)\sin(\theta)\sin(\phi) + \cos(\psi)\cos(\phi)) + w(\sin(\theta)\sin(\psi)\cos(\phi) - \cos(\psi)\sin(\phi)) \\ \dot{h} &= u\sin(\theta) - v\cos(\theta)\sin(\phi) - w\cos(\theta)\cos(\phi) \end{aligned} \tag{4}$$

The Eq. (1) - (4) are the complete set of the kinematic non-linear relationship. However, just altitude h is used, because is the only position state that has any bearing on the aircraft stability and control (because air density varies with altitude), so the kinematics equations associated with x_E and y_E are generally not used.

With the kinematic defined it is fairly straightforward to derive other variables Gomes Pereira Sarmento *et al.* (2019), angles of attack α and sideslip β, the true airspeed V and dynamic pressure $\bar{q}$.

$$\begin{aligned} \alpha &= \tan^{-1}\left(\frac{w}{u}\right) \\ \beta &= \sin^{-1}\left(\frac{v}{V}\right) \end{aligned} \tag{5}$$

where the angles of attack α and sideslip β, are express in function of the translational speeds u, v, w and the true airspeed V.

$$V = \sqrt{(u^2+v^2+w^2)} \tag{6}$$

The true airspeed V, written in the function of the transnationals speeds u, v, w.

$$\bar{q} = \frac{1}{2}\rho V^2 \tag{7}$$

in Eq. (7) for the dynamic pressure $\bar{q}$, it is admitted the air density ρ may be assumed constant if the variations in altitude during the test maneuver are small and can be obtained from standard atmosphere tables.

3 FLIGHT TEST

The flight test was realized in September 2020. The flight test was executed with a series of maneuvers with the purpose to excite the flexible modes of the UAS. To do that, it is necessary to input a specific perturbation in the equilibrium position, this perturbation is given by a fast input command (impulse) at the control surface, for example, if is desired to excite the longitudinal flexible modes, is just input a fast command (impulse) in the elevator when the aircraft is in an equilibrium position. This quick command has a minimum finite duration of Δt, in the sense of creating an impulse sign like shown in Figure (3). Then for a better excitation is possible to use a multi-step signal.

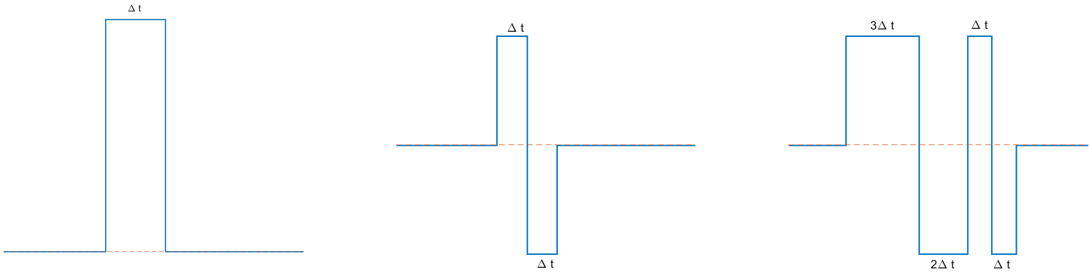

Figure 3 – Inputs signals: pulse, doublet and multistep $3-2-1-1$**.**

The multi-step signal can be synthesized by a sequential combination of impulse inputs. For this type of signal have the power spectrum given by Zúñiga *et al.* (2019a):

$$E(\omega) = 2\Delta t^2 \frac{1-cos(\Omega)}{\Omega^2}\left[\sum_{i=1}^{N} V_i^2 + 2\sum_{j=1}^{N-1} cos(j\Omega)\sum_{i=1}^{N-j} V_i V_{i+j}\right] \tag{8}$$

where $\Omega = \omega\Delta t$ is the normalized frequency, $T = N\Delta t$ the total time of the input signal, considering N impulses each of configuration Δt, and V_i is the amplitude for the current impulse, the Fig.4 illustrate this equation for four types of inputs: pulse, multi-step $3-2-1-1$ and modified multi-step $3-2-1-1$.

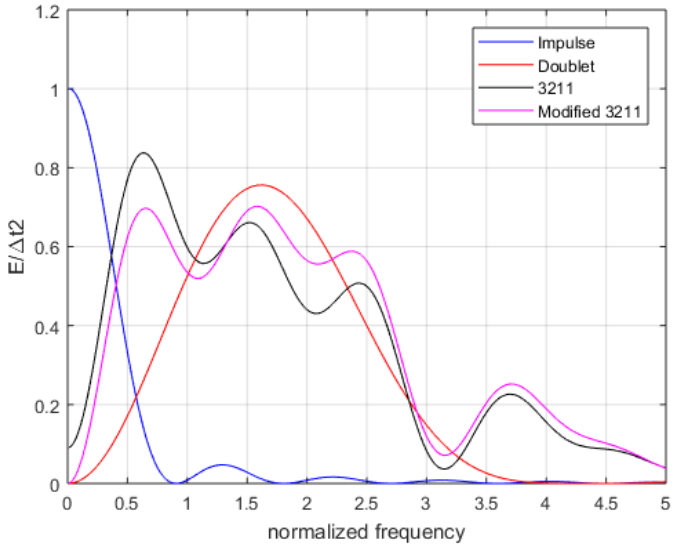

Figure 4 – Spectrum of the different input.Zúñiga *et al.* (2019a)

The Δt can be obtained by the expressions for a Doublet (two impulses on opposite sides).

$$\Delta t_{doublet} = \frac{2.3}{\omega_n} \tag{9}$$

for the multistep $3-2-1-1$ existed two possibilities:

$$\textbf{(a)}\ \Delta t_{3211a} = \frac{1.6}{\omega_n} \quad \textbf{(b)}\ \Delta t_{3211b} = \frac{2.1}{\omega_n} \tag{10}$$

in the Eq. (9) and 10 (a,b) ω_n is the natural frequency. In a way to excite a specific frequency is possible to use the relation Zúñiga *et al.* (2019a):

$$\Delta t_{3211sp} = \frac{0.3}{f_c} \tag{11}$$

where f_c is the desired frequency to be excited.

In the article Castillo et al. (2019) Zúñiga *et al.* (2019a) it was deduced the Δt for a set of flexible modes.

3.1 Data Flight

Due to some technical issues, is very difficult for the pilot to give these inputs in the radio controller available. Then, the maneuvers were done by having a set with $\Delta t = 0.5\ s$ and another set with a non-measured Δt but, done faster than the pilot can do.

A camera was installed in the wing of the UAS with the objective to film the flexibility of the wing during the flight test.

Figure 5 – Two different frames, the upper picture is an equilibrium position and above a flexible excitation.

Figure (5) shows an equilibrium condition (upper) and a flexible deformation of the semi-wing.

It was realized two flights with a duration of 30 minutes each. On the day of tests, it was sunny, but with gusts of wind, for that, the UAS was all the time in a pilot-in-the-loop condition. The maneuvers were made in a sequence of 3 sets of 3-2-1-1 input, with a Δt equals a 0.5 s for every one control surface and 3 sets with the same strategy but, with an undetermined Δt (based on the more fast input that can be possible by the pilot).

For this study was select a time set of 60 s this time set has three doublets input in the elevator and a right turn.

Figure (6) shows the data record used for this study. The variables ploted are: V airspeed measured by the Pitot tube in m/s, the Euler's angle (θ, ϕ and ψ) measured in deg, the rotational velocities (p, q and r) measured in deg/s and the accelerations (ax, ay and az) measured in m/s^2.

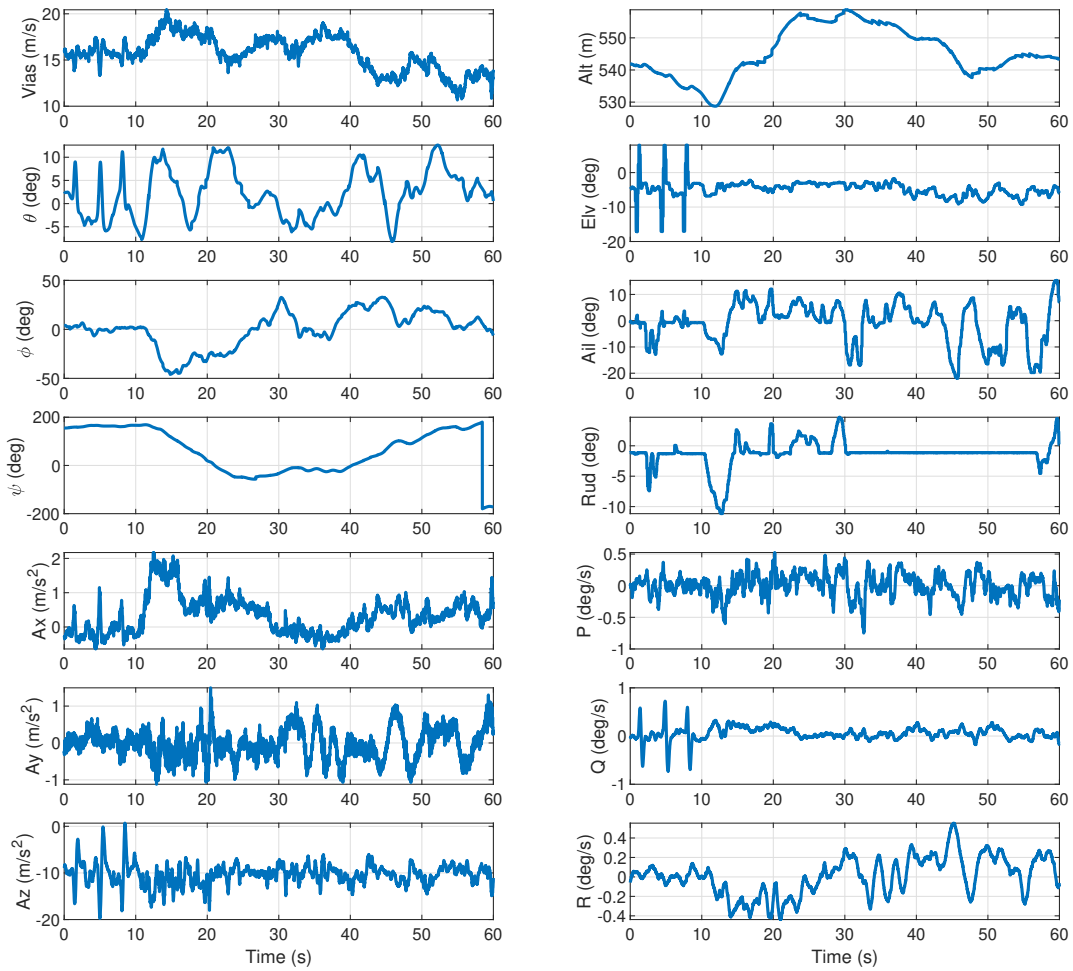

Figure 6 – Data set for the FPR

4 OUTPUT ERROR METHOD (OEM)

Since the effects of flight configuration under operating conditions cannot be tested realistically in a laboratory, calibration from flight data is necessary to eliminate the errors. A way to make a correction in the measurement data is admitting a simple sensor model in terms of scale factor, bias, and time delay, for any general measurement variable y_m Hamel and Jategaonkar (1996), which can be expressed as:

$$y_m = F_y y(t-\tau) + \Delta y \tag{12}$$

where τ is the time delay in the recorded signal, Δy the unknown instrument bias and F_y is calibration factor Hamel and Jategaonkar (1996). The instrument error is considered constant over all the recorded data. The sensor model given in Eq. (12) can be applied to input and output variables.

For the FPR and consequently for the data compatibility check is necessary to make the estimation of the bias and factor scale of the output variables. The estimation process is made using the output error method (OEM) Hamel and Jategaonkar (1996).

In this class of output error methods, the model parameters are adjusted iteratively to minimize the error between the measured variables (system output) and the estimated responses (predicted measures of the nonlinear model), Kamali and Ozger (2019) Souza *et al.* (2018) for this ratio it is enough to minimize the maximum likelihood function so that:

$$\hat{\Theta} = arg\left\{\max_{\Theta} \ln(p(z|\Theta))\right\} \tag{13}$$

Admitting Θ as the parameters vector and $z = [z_1, z_2, \ldots, z_N]$ the set of observations and p the probability of z such that Θ occurred.The likelihood function can be defined as conditional probability density $p(z(t_1), \ldots, z(t_N)|\Theta, R)$ with n_y measured from a vector with N points sampled for a given parameter vector Θ, with the covariance error measure matrix R Souza *et al.* (2018) Hamel and Jategaonkar (1996). The conditional probability density of the measurements t_k is given by:

$$p[z(t_k)|\Theta, R] = \frac{1}{(2\pi)^{n_y/2}\sqrt{|R|}} \times exp\left[-\frac{1}{2}\{z(t_k)-y(t_k)\}^T R^{-1}\{z(t_k)-y(t_k)\}\right] \tag{14}$$

y is the measured vector (model output - *model output*). Having the error $\nu(t_k) = z(t_k) - y(t_k)$ at different time moments should be statically independent.

From the equation Eq. (14) we can immediately calculate the maximum likelihood estimates of the unknown parameters Θ and the covariance matrix of the measurement noise R, establishing the first derivatives in relation to each of them and equaling them to zero. However, an equivalent and more practical solution to the optimization problem is the minimization of $L(z|\Theta, R)$ is the use of the negative logarithm of the likelihood function Hamel and Jategaonkar (1996).

$$J(\Theta, R) = L(z|\Theta, R) = \frac{1}{2}\sum_{k=1}^{N}[z(t_k)-y(t_k)]^T R^{-1}[z(t_k)-y(t_k)] + \frac{1}{2}ln(det(R)) + \frac{Nn_y}{2}ln(2\pi) \tag{15}$$

The result of the $\partial(lnp)/\partial\Theta = 1/p \cdot \partial p/\partial\Theta$ differs ensures that the *log* derivative of p is zero when $\partial p/\partial\Theta$ is zero and thus produces the same results Hamel and Jategaonkar (1996). The last term in Eq. (15) is a constant and therefore neglected in optimization without affecting the results. The cost function can be written as:

$$J(\Theta, R) = \frac{1}{2}\sum_{k=1}^{N}[z(t_k)-y(t_k)]^T R^{-1}[z(t_k)-y(t_k)] \tag{16}$$

That simplification brings a discussion about the covariance matrix R. If the matrix R is known, then the optimization resumes a least square problem, but if the matrix R are unknown the optimization of Eq. (16) leads to a new cost function,

$$J(\Theta) = \frac{N}{2}ln(det(R)) \quad \rightarrow \quad J(\Theta) = det(R) \tag{17}$$

Now the optimization problem that consists of finding Θ that minimizes $J(\Theta)$, for this is possible use different methods, for this is possible to use different methods, for this problem it was used the Gauss-Newton optimization algorithm Hamel and Jategaonkar (1996).

5 COMPUTATIONAL RESULTS AND BIAS ESTIMATION

Using the kinematics equations shown in the previous section 2.1 and the OEM approach presented in section 4, a computational MatLab software is developed to propagate the kinematic equations and estimate the bias and the scale factor of the anemometer.

For the input variables p, q and r and a_x, a_y and a_z are measured by the inertial sensors in board and they are shown in Figure (6), now the other three variables $\dot{p}$, $\dot{q}$ and $\dot{r}$ are calculated using a numerical differential procedure using the data of p, q and r.

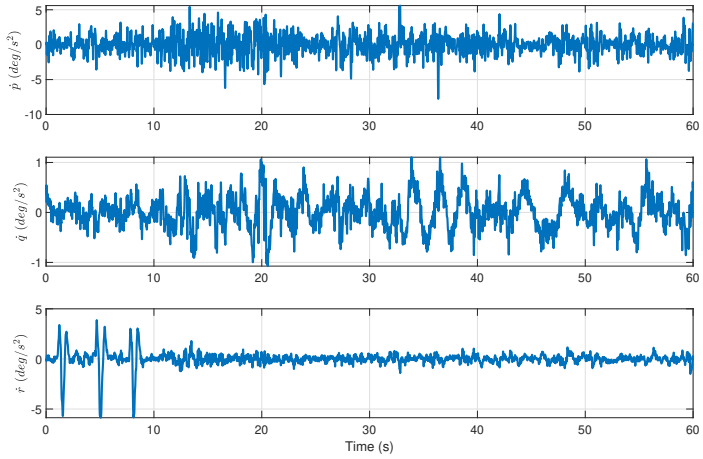

Figure 7 – Calculated $\dot{p}$, $\dot{q}$ and $\dot{r}$

Figure (7) the calculated variables $\dot{P}$, $\dot{Q}$ and $\dot{R}$ are presented. For this set of calculated data, it is considered whit no systematic error.

Then the output variables are integrated, and they are the Euler angles (θ, ϕ and ψ), angles of attack and sideslip (α and β), the airspeed and altitude (h).

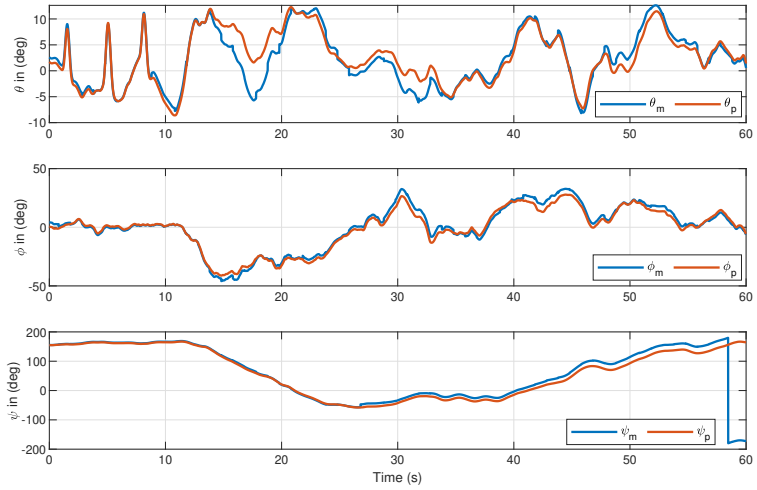

Figure 8 – Euler angles measured x propagate

Figure(8) shows the three Euler angles (θ, ϕ and ψ), the line red is the propagate states and the blue line is the measured states. Looking at the first 10 s, exists a good match of the data. The importance of the firsts 10 s is done because is in this interval that occurs the three sequences of elevator doublet.

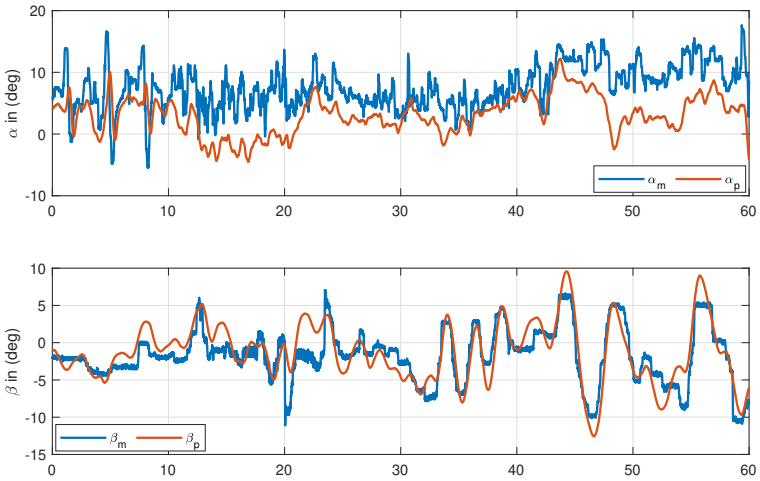

Figure 9 – Angles of Attack and sideslip measured x propagate

Now, Figure (9) shows the angle of attack (AOA - α) and sideslip (AOS - β), the red line is the propagate states and the blue line is the measured states. Again looking for the first 10 s, the estimated AOA does not have a good match with the measured one, but they have a synchronous reaction to the moving parts, whereas the AOS does not have any match between the two curves. These results indicate that this set of data is only going to be useful for a longitudinal dynamic identification.

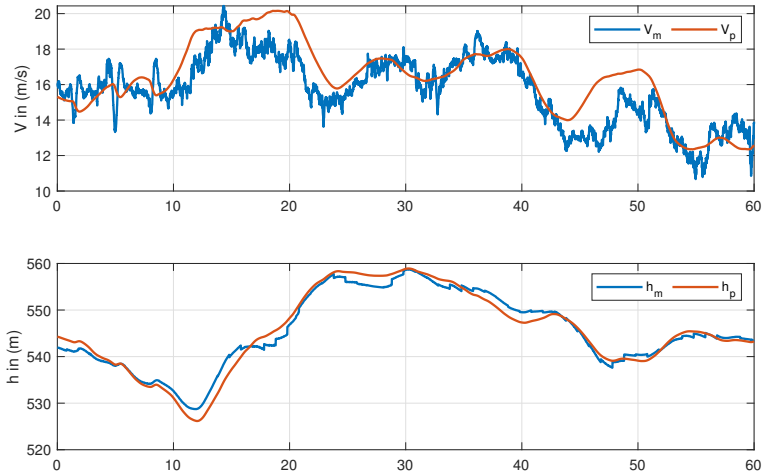

Figure 10 – Altitude and airspeed measured x propagate

Figure (10) shows the airspeed and altitude are propagated. The red line is the propagated answer and the blue line is the measured data. The airspeed (V) in the estimated case doesn't converge to the real measurement and for altitude (h), in the 10 s first seconds the estimated curve follows the same comportment to the measure estimated

This data set propagated is shown in the Figures (8) - (10) also includes a bias correction and a doesn't factor.

Figure (11) shows the estimated bias for the state variables p, q, r and a_x, a_y, a_z in function of the iteration number.

The results given by this analysis indicate (for this data set) useful sensors in the longitudinal axes (around the xz plane, in the body reference) have better accuracy than that in the lateral-directional axes.

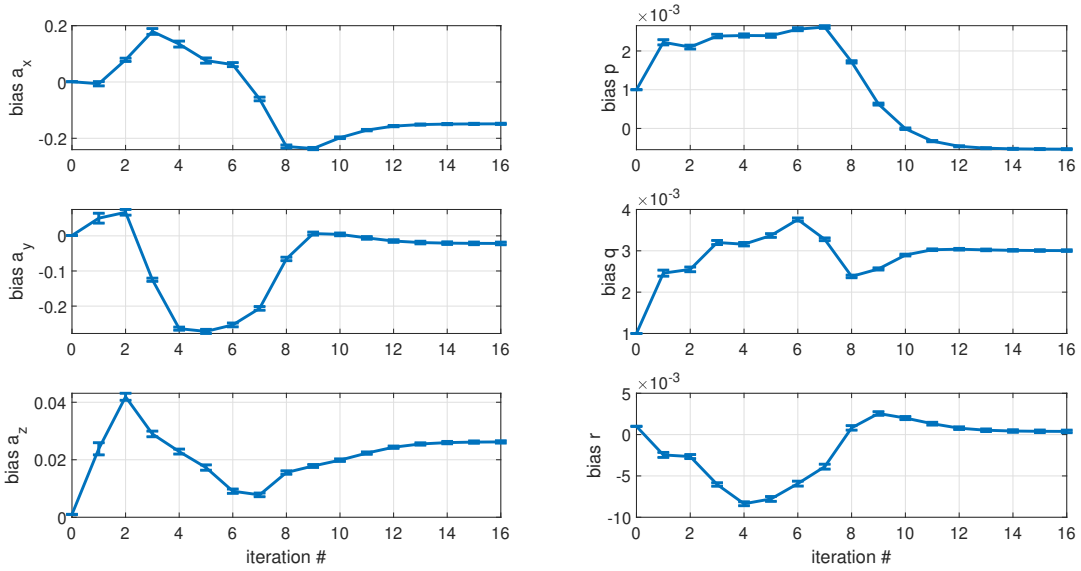

Figure 11 – Bias of the states p, q, r and a_x, a_y, a_z

For this data compatibility, one can conclude that this data set, is possible to be used for a longitudinal identification process.

6 CONCLUSION

This paper is based on a part of ongoing research with the proposition of these study the influence of the flexibility dynamics in the Eolo configurations and identifying the aerodynamic derivatives, of this UAS.

This paper showed a compatibility check, that consists to make the FRP of the flight data and estimate the angular and wind variables. This procedure it was showed the flight test campaign, the mathematical equations for the kinematic movement, and the state estimate using the OEM.

The results of the computational analysis permit us to estimate the rotational states, speeds, and altitude. It seems that the first assumption made in the kinematic equations was violated due, probably, to the wing flexibility, by the other side if these assumptions are not made is not possible to execute the FRP, useful aerodynamics forces present in Eq. (1) has his parameters are unknown.

Exist numerical methods to estimate these aerodynamic parameters, but if don't realize the study admits a rigid system is not possible to understand how this dynamic acts in the system and if the sensors measurements are correct by a model pre-defined when the data is used in an identification process, naturally the systems go converge to this pre-defined model, and that no guarantees that these values equal to the real values.

The longitudinal identification was made a new study, in a sense of data compatibility check, can be executed with the proposes to investigate the influence of the wing flexibility in the lateral-directional aerodynamic and a more robust wind estimation can be integrated into the system for the FPR.

ACKNOWLEDGMENTS

The authors are grateful for the funding of CAPESwered FINEP/VINNOVA, the partnership between Flight Technologies and ITA. To the team of the Measurement of mass proprieties laboratory (IAE) and in special to Ciro V. who piloted the UAS in the Flight tests.

The authors acknowledge the support given by FCT, through IDMEC, under LAETA project UID/EMS/50022/2020.

REFERENCES

Barbosa, R.C.M.G. and Góes, L.C.S., 2018. "Closed-loop system identification of a large flexible aircraft using subspace methods". *31st Congr. Int. Counc. Aeronaut. Sci. ICAS 2018*, pp. 1–9.

de Oliveira Silva, B.G., 2011. "Data gathering and preliminary results of the system identification of a flexible aircraft model". *AIAA Atmos. Flight Mech. Conf. 2011*, , No. August, pp. 1–24. doi:10.2514/6.2011-6355.

de Oliveira Silva, B.G. and Mönnich, W., 2012. "System identification of flexible aircraft in time domain". *AIAA Atmos. Flight Mech. Conf. 2012*, , No. August, pp. 1–26. doi:10.2514/6.2012-4412.

De Silva, A.L., Paglione, P. and Yoneyama, T., 2010. "Conceptual flexible aircraft model for modeling, analysis and control studies". *AIAA Atmos. Flight Mech. Conf. 2010*, , No. August. doi:10.2514/6.2010-7806.

Dias, J.N., 2014. "Flight path reconstruction techniques applied to spin tests". *AIAA Aviat. 2014 -AIAA Atmos. Flight Mech. Conf.*, , No. June, pp. 1–12. doi:10.2514/6.2014-2559.

Gomes Pereira Sarmento, A., Souza, A., Castillo Zuñiga, D.F. and Sandoval Góes, L.C., 2019. "SYNTHETIC ESTIMATION OF ANGLE OF ATTACK AND SIDESLIP FOR FLIGHT TESTING OF AN UNMANNED AERIAL VEHICLE". In *Proc. 25th Int. Congr. Mech. Eng.* ABCM. doi:10.26678/ABCM.COBEM2019.COB2019-1578. URL http://abcm.org.br/anais-de-eventos/COB2019/1578.

Hamel, P.G. and Jategaonkar, R.V., 1996. "Evolution of flight vehicle system identification". *J. Aircr.*, Vol. 33, No. 1, pp. 9–28. ISSN 15333868. doi:10.2514/3.46898.

Kamali, C. and Ozger, E., 2019. "Limitations of Flight Path Reconstruction techniques". *Sadhana - Acad. Proc. Eng. Sci.*, Vol. 44, No. 2, pp. 1–15. ISSN 09737677. doi:10.1007/s12046-018-1019-3. URL https://doi.org/10.1007/s12046-018-1019-3.

Martínez, A.V., Boschetti, P.J. and González, P.J., 2020. "Dynamic stability and flying qualities of an unmanned airplane as a flexible body". *AIAA Scitech 2020 Forum*, Vol. 1 PartF, No. January, pp. 1–14. doi:10.2514/6.2020-1268.

Pfifer, H. and Danowsky, B., 2016. "System identification of a small flexible aircraft". *AIAA Atmos. Flight Mech. Conf.*, , No. January, pp. 1–14. doi:10.2514/6.2016-1750.

Souza, A., Castillo Zuñiga, D.F. and Sandoval, L.C., 2019. "Parameter Identification for a Flexible Unmanned Aerial Vehicle Using Extended Kalman Filtering". In *DINAME2019*. ABCM. doi:10.26678/ABCM.DINAME2019.DIN2019-0192. URL http://abcm.org.br/anais-de-eventos/DIN2019/0192.

Souza, A., Goes, L., Sousa, M., Zuñiga, D. and Barbosa, R., 2018. "Identificação de parâmetro da dinâmica longitudinal de uma aeronave flexível usando o método de erro na saída." doi:10.26678/ABCM.CONEM2018.CON18-1379.

Theis, J., Pfifer, H., Balas, G. and Werner, H., 2015. "Integrated flight control design for a large flexible aircraft". *Proc. Am. Control Conf.*, Vol. 2015-July, pp. 3830–3835. ISSN 07431619. doi:10.1109/ACC.2015.7171927.

Waszak, M.R. and Schmidt, D.K., 1988. "Flight dynamics of aeroelastic vehicles". *J. Aircr.*, Vol. 25, No. 6, pp. 563–571. ISSN 00218669. doi:10.2514/3.45623.

Zúñiga, D.F.C., Souza, A.G. and Góes, L.C.S., 2019a. "Planning of an in-Flight Aeroelastic Testing of a Flexible Unmanned Aerial Vehicle Using a Combined Accelerometers-Strain Sensors Operational Modal Analysis". In *Int. Conf. Struct. Eng. Dyn. ICEDyn 2019*. Viana do Castelo, PT.

Zúñiga, D.F., Souza, A.G. and Góes, L.C., 2019b. "Development of an aeroelastic in-flight testing system for a flexible wing unmanned aerial vehicle using acceleration and strain sensors". *AIAA Scitech 2019 Forum*, , No. January. doi:10.2514/6.2019-2033.

RESPONSIBILITY NOTICE

The authors are the only ones responsible for the printed material included in this paper.